Geophysical Journal International

Geophys. J. Int. (2016) **205,** 284–300
GJI Gravity, geodesy and tides

doi: 10.1093/gji/ggw017

Temporal variation of tidal parameters in superconducting gravimeter time-series

Bruno Meurers,[1] Michel Van Camp,[2] Olivier Francis[3] and Vojtech Pálinkáš[4]

[1]*Department of Meteorology and Geophysics, University of Vienna, Austria. E-mail: bruno.meurers@univie.ac.at*
[2]*Royal Observatory of Belgium, 3 avenue Circulaire, B-1180 Brussels, Belgium*
[3]*Faculté des Sciences, de la Technologie et de la Communication, University of Luxembourg, 6, rue Richard Coudenhove-Kalergi, L-1359 Luxembourg*
[4]*Research Institute of Geodesy, Topography and Cartography, Geodetic Observatory Pecný, Czech Republic*

Accepted 2016 January 12. Received 2016 January 8; in original form 2015 September 25

SUMMARY

Analysing independent 1-yr data sets of 10 European superconducting gravimeters (SG) reveals statistically significant temporal variations of M2 tidal parameters. Both common short-term (<2 yr) and long-term (>2 yr) features are identified in all SG time-series but one. The averaged variations of the amplitude factor are about 0.2‰. The path of load vector variations equivalent to the temporal changes of tidal parameters suggests the presence of an 8.85 yr modulation (lunar perigee). The tidal waves having the potential to modulate M2 with this period belong to the 3rd degree constituents. Their amplitude factors turn out to be much closer to body tide model predictions than that of the main 2nd degree M2, which indicates ocean loading for 3rd degree waves to be less prominent than for 2nd degree waves within the M2 group. These two different responses to the loading suggest that the observed modulation is more due to insufficient frequency resolution of limited time-series rather than to time variable loading. Presently, SG gravity time-series are still too short to prove if time variable loading processes are involved too as in case of the annual M2 modulation known to appear for analysis intervals of less than 1 yr. Whatever the variations are caused by, they provide the upper accuracy limit for earth model validation and permit estimating the temporal stability of SG scale factors and assessing the quality of gravity time-series.

Key words: Time-series analysis; Time variable gravity; Tides and planetary waves; Europe.

1 INTRODUCTION

The amplitude factor and phase lag tidal parameters derived from gravity data are useful to validate or discriminate between different body tide models (e.g. Baker & Bos 2003; Ducarme *et al.* 2014), provided the transfer function of the gravimeter is known with sufficient accuracy. The quality of ocean models, which are indispensable for correcting for the ocean load effects (e.g. Bos & Baker 2005), is another limitation of the validation process. Nowadays, the scale factor of superconducting gravimeters (SGs) can be determined with a precision level better than 1‰ (e.g. Francis *et al.* 1998; Hinderer *et al.* 2007). The instrumental time lag of the system can be determined with a precision of 0.01 s (Van Camp *et al.* 2000). The SG amplitude factor is derived mostly from colocated absolute gravimeter observations. However, results of repeated calibration experiments can differ by more than 1‰ (e.g. Rosat *et al.* 2009; Meurers 2012; Virtanen *et al.* 2014). Averaging over several experiments allows for determining a robust scale factor with error even below the 1‰ level (Rosat *et al.* 2009, Virtanen *et al.* 2014) provided the SG scale factor remains stable. Seven experiments are required to ensure calibration accuracy at the 1‰ level with 99 per cent confidence (Van Camp *et al.* 2016). Non-detected temporal changes of the gravimeter transfer function are basically reflected by temporal variations of tidal parameters, which, however, might be caused also by other reasons as discussed below. Analysing newer independent data sets of 1-yr coverage exhibits clearly temporal variations of the associated tidal parameters (e.g. Calvo *et al.* 2014; Meurers *et al.* 2014). Calvo *et al.* (2014) investigated the time stability of spring and superconducting gravimeters by analysing very long gravity records. They did not find a clear correlation between time variations of amplitude factors while a preliminary analysis by Meurers *et al.* (2014) suggests that for M2 similar patterns can be identified at most of the SG sites.

Temporal variations of tidal parameters may have different causes:

(1) *Calibration:* Temporal instability of the gravimeter scale factor due to, for example, improper performance of the tilt compensation device or changes of electronics. However, it is unlikely that scale factor variations of different SG instruments, if present, occur such that they produce common variability in the tidal parameters.

(2) *Pre-processing:* Undetected offsets and/or spikes in the gravity data deteriorate the quality of the frequency spectra. In addition, excessively filling gaps by wrong model tides may explain

anomalous features at a specific site within a specific period. Again, it is unlikely to find such features coherently appearing at different stations.

(3) *Numerical artefacts due to insufficient frequency resolution in tidal analysis:* Tidal analyses are always based on limited time-series. Therefore, it is impossible to separate all constituents of the discrete tidal spectrum. Instead, the constituents are combined into groups assuming the tidal parameters being equal within a specific group. This concept fails if tidal parameters do not smoothly vary with frequency, for example in case of non-linear effects [e.g. Merriam 1995, see point (4)], or if 2nd and 3rd degree constituents with different response to ocean loading mix up. Variations in the tidal parameters have been studied for a long time (e.g. Chojnicki 1989; Dittfeld 1989) and turned out to be mainly caused by inseparable 3rd degree constituents within the tidal groups (Dittfeld 1991). In addition, former results were clearly deteriorated by instrumental noise. In modern tidal analysis codes, this problem has been solved (Wenzel 1996) to large extent, namely for the response of the elastic Earth by introducing *a priori* amplitude factors from global models (e.g. Dehant 1987) for tidal waves of different degree and order. However, this procedure does not consider different response to ocean load within a group, if present. Fig. 1 presents the tidal spectrum of the Hartmann & Wenzel (1995a) tidal potential catalogue around the M2 group with amplitudes normalized to M2 taking the fully normalized Legendre polynomials for northern mid-latitudes into account (Hartmann & Wenzel 1995b). When analysing 1-yr intervals we cannot separate reliably the constituents GAM2, MA2, MB2 and DLT2 from the main M2. However, this does not matter because the analysis interval of 1-yr is almost an integral multiple of their associated modulation periods (see Appendix A and modulation periods displayed in Fig. 1). Next to M2, some constituents exist with considerable amplitude, which are able to cause the 18.6 yr nodal modulation (2nd degree wave 255.545) as well as the lunar perigee modulation with periods of about 8.85 yr (3rd degree waves 255.455 and 255.655; Fig. 1). Details on the tidal waves with the largest amplitude in their group are reported in Appendix B showing also the degree of the tidal potential they stem from (Table B1). Darwin symbols do not exist for the M2 satellites; therefore we make use of the Doodson arguments to discriminate additional wave groups on both sides of M2. In addition, Appendix B presents examples of how modulation effects can be generated in tidal analyses.

(4) *Temporal variation of the ocean load:* Based on tide gauge data around Great Britain, Baker & Alcock (1983) identified seasonal variations in the main tidal groups. Huess & Andersen (2001) investigated sea level variations in the North Sea based on altimetry data. They identified the seasonal M2 variation as caused by shallow water effects which modify the amplitudes of the constituents MA2 and MB2. Hydrodynamic modelling showed that a large part of this variation could be explained by meteorological forcing. Müller *et al.* (2014) studied the seasonal M2 variations globally by analysing ocean circulation and tide model simulation as well as observed satellite altimeter and tide-gauge data. For coastal regions of the North Sea they quantified the seasonal M2 variations ranging up to 0.05 m. Gräwe *et al.* (2014) interpret them as being caused by the thermal structure of the North Sea varying along the seasons. Tide gauge data obtained at marine coasts show significant trends or secular changes in the M2 water tide amplitude. They were proven to exist in the North Atlantic Sea (e.g. Cartwright 1972; Amin 1985; Müller 2011; Müller *et al.* 2011) as well as in other regions (e.g. Ray 2006; Woodworth 2010). These findings suggest that temporal changes in the ocean loading pattern cannot be excluded.

(5) Tidal parameters predicted by global body tide models (e.g. Dehant *et al.* 1999) depend on the radial distribution of density and Lame's parameters within the entire Earth. Métivier & Conrad (2008) recently studied the role of lateral heterogeneities. In all

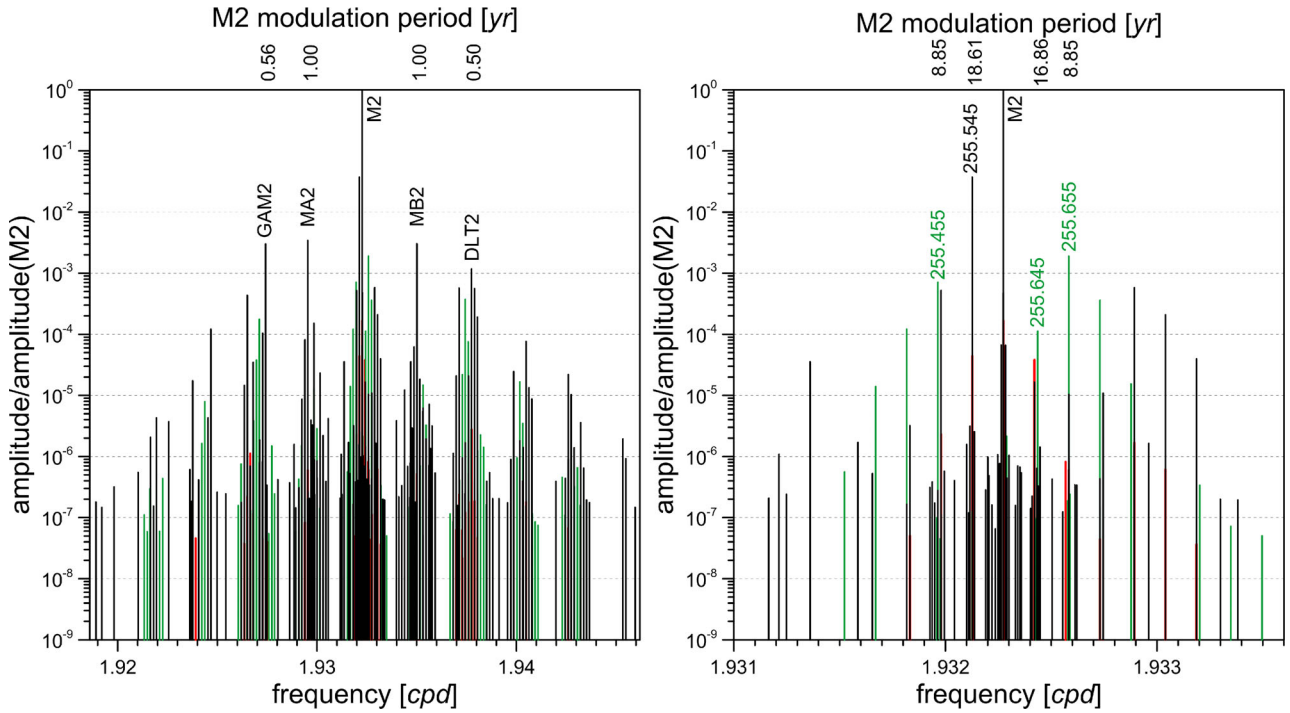

Figure 1. Tidal spectrum of the Hartmann & Wenzel (1995a) tidal potential catalogue next to the M2 group (left-hand side) and fine structure close to M2 (right-hand side). The top axis indicates the periods of the M2 modulation caused by constituents if they are not properly separated in tidal analysis. 2nd degree waves in black, 3rd degree waves in green, 4th and 5th degree in red.

Table 1. Location of SG sites, instrumentation and length of gravity time-series.

SG	Location	Latitude (°N)	Longitude (°E)	Height (m)	SG type	Length of records
BH1	Bad Homburg (Germany)	50.2285	8.6113	190.0	CD030_L	2001 Feb–2007 Mar
BH2					OSG-044	2007 Feb–2013 Oct
CO	Conrad Observatory (Austria)	47.9283	15.8598	1045.0	CT-025	2007 Nov–2012 Oct
MB	Membach (Belgium)	50.6085	6.0095	250.0	CT-021	1998 Jun–2013 Aug
MC	Medicina (Italy)	44.5219	11.6450	28.0	CT-023	1998 Jan–2012 Jan
MO	Moxa (Germany)	50.6447	11.6156	455.0	CD-034L	2000 Jan–2011 Dec
PE	Pecný (Czech Republic)	49.9138	14.7856	534.6	OSG-050	2007 May–2013 Jul
ST	Strasbourg (France)	48.6217	7.6838	180.0	CT-026	1997 Mar–2012 May
VI	Vienna (Austria)	48.2489	16.3565	192.0	CT-025	1995 Aug–2007 Oct
WA	Walferdange (Luxembourg)	49.6647	6.1528	295.0	OSG-040	2003 Dec–2013 Dec
WE	Wettzell (Germany)	49.1440	12.8780	613.7	CD-029U	1998 Nov–2010 Oct

these aspects, we do not expect temporal changes on subgeological time scales. On the other hand, based on synthetic model studies, Beaumont & Berger (1974) show that tectonic processes associated with *P*-wave velocity changes can play an important role in modifying tidal radial displacement, tilt and strain above a spatially limited dilatant region. If such signals were strong enough to be seen in tidal gravity, they would be restricted to a limited area and not expected to be seen coherently at distant stations.

Thus, common features in the temporal evolution of tidal parameters for specific tidal constituents strongly suggest physical processes associated with time-varying loading or numerical issues like modulations related to the frequency resolution problem in tidal analysis. On the other hand, whatever the reasons are, investigation of tidal parameter variations is a suitable tool for evaluating the temporal stability of SG scale factors (Calvo *et al.* 2014) and for identifying disturbed observation periods. It is also a way to assess the accuracy limit of earth model validation under the optimum condition of perfectly calibrated instruments.

Here, we investigate temporal variations of tidal parameters observed at 10 European stations equipped with superconducting gravimeters (Table 1 and Fig. 2): Bad Homburg (BH), Conrad observatory (CO), Medicina (MC), Membach (MB), Moxa (MO), Pecný (PE), Strasbourg (ST), Walferdange (WA), Wettzell (WE) and Vienna (VI) with observation periods between 5 and 15 yr. CO, PE, VI and WE represent intracontinental sites, while MB and MC are closer to the Atlantic Ocean and Mediterranean/Adriatic Sea, respectively.

VI and CO are the only sites occupied by the same SG. For more than 12 yr, the SG GWR C025 was installed in an underground laboratory in VI and moved to Conrad observatory (CO) 60 km SW of Vienna in autumn 2007. The SG sphere was kept levitated during transport. Consequently, only minor re-adjustment measures were required, among others because of the gravity difference between both sites. Numerous calibration experiments proved that the SG scale factor did not change significantly due to the transfer of the SG from VI to CO and its re-installation (Meurers 2012), while the time lag changed actually by about 0.4 *s*. The BH time-series refers to two different SGs due to an instrumental upgrade in 2007.

Processing of the original 1 *s* SG data consists of calibration by the SG scale factor, degapping, destepping, despiking and decimation to 1 hr samples (e.g. Hinderer *et al.* 2007). This is a crucial process as wrong calibration parameters, hidden offsets or spikes deteriorate the entire spectrum and consequently the tidal analysis result. Gravity data of the stations MB, WA, VI, CO and PE were obtained directly from the operators while BH, MC, MO, ST and WE were processed by the International Centre for Earth Tides (ICET) and provided by the Information System and Data Centre (ISDC) of the German Research Centre for Geosciences—GFZ (http://isdc.gfz-potsdam.de/). In the first case, we can trust that all processing steps have been done based on best knowledge of the calibration history and technical issues causing offsets or other distortions.

2 TIDAL ANALYSIS

Using the Hartmann & Wenzel (1995a) tidal potential catalogue, we analyse successive and overlapping intervals of 3 months and 1 yr by shifting the data window over the gravity time-series in steps of 15 and 30 d, respectively. Tidal parameters for groups combining inseparable constituents as well as the air pressure admittance factors in the diurnal and subdiurnal frequency bands are adjusted by applying ETERNA v3.4 (Wenzel 1996). The load vectors for the correction of the ocean loading effect are provided by the Free Ocean Tide Loading Provider (Bos & Scherneck 2014) based on eight different global ocean tide models: CSR4.0 (Eanes 1994), GOT00.2 (Ray 1999), TPXO7.2 (Egbert & Erofeeva 2002), FES2004 (Lyard *et al.* 2006), EOT11a (Savcenko & Bosch 2011), DTU10 (Cheng & Andersen 2010), HAMTIDE (Taguchi *et al.* 2010) and NAO99 (Matsumoto *et al.* 2000). Finally, we calculate the corrected tidal parameters for the M2 and O1 constituents at each SG station by averaging the results of the eight ocean models because the latter differ from model to model especially at locations in coastal areas (e.g. Habel & Meurers 2014) due to the limited spatial resolution of the models. We apply this correction step just routinely: we do not intend to validate body tide models in this paper.

Analysis on 3 months

Both the M2 amplitude factors and phases derived from the 3-months periods show a clear annual variation which disappears when analysing 1-yr intervals. This well-known phenomenon is due to anomalous amplitude factors of the MA2 and MB2 constituents within the M2-band as shown, for example for the Bay of Fundy and the east coast of North America (Merriam 1995). If all constituents of a same degree had the same amplitude factor, no modulation would be observed (see Appendices A and B). In the frequency spectrum both the MA2 and MB2 constituents are close to M2 with a frequency difference of about 0.04107 deg hr^{-1} (Fig. 1). As they cannot be separated in the tidal analysis of 3-months intervals, an annual modulation of M2 appears (see also Appendix B). When the time-series is long enough for separating both constituents, their amplitude factors turn out to be significantly higher than expected (e.g. Meurers 2004). In Table 2, this is shown for the SG time-series exceeding 10 yr.

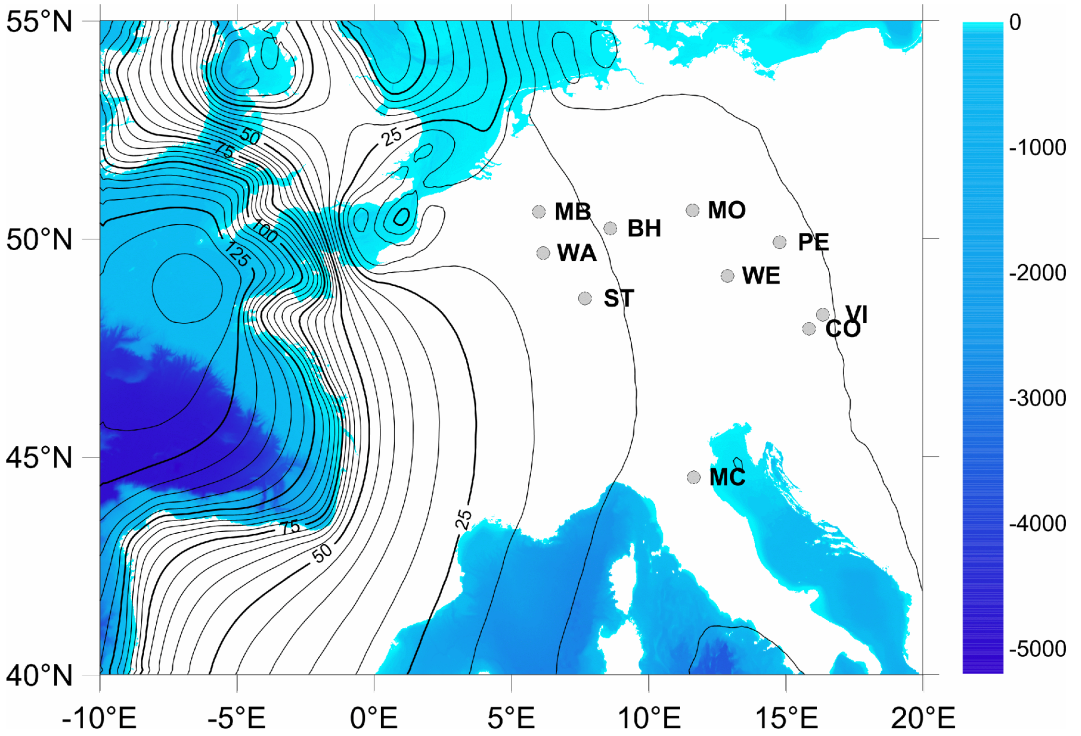

Figure 2. Location of the SG stations and amplitude [nms^{-2}] of the M2 ocean load. Colours indicate the ocean depth (m) based on the global 30 arcsec grid GEBCO_2014 (http://www.gebco.net/).

Table 2. Amplitudes (A) (nms^{-2}) and potential degree d, amplitude factors δ and phases κ (°) and their standard deviations σ resulting from tidal analysis for the tidal groups next to M2, performed on SG series longer than 10 yr.

Frequency (cpd)											
from	to		d		MB	MC	MO	ST	VI	WA	WE
1.928403	1.930700	MA2	2	A	1.0405	1.3128	1.0389	1.1288	1.1455	1.0822	1.1055
				δ	**1.21412**	**1.19133**	**1.20280**	**1.21558**	**1.19092**	**1.21601**	**1.19857**
				σ_δ	0.00454	0.00504	0.00533	0.00461	0.00351	0.00452	0.00533
				κ	1.0620	–0.5422	0.1075	0.3870	–0.3569	0.8509	–0.2168
				σ_κ	0.2140	0.2426	0.2539	0.2174	0.1690	0.2128	0.2550
1.930701	1.932099	255.455	3	A	0.3229	0.3694	0.3225	0.3400	0.3431	0.3312	0.3357
				δ	**1.07427**	**1.10893**	**1.06743**	**1.07813**	**1.07542**	**1.07741**	**1.18761**
				σ_δ	0.01156	0.01361	0.01324	0.01163	0.00888	0.01194	0.01349
				κ	0.0299	2.0732	–0.4724	1.1248	1.5397	–0.8099	–1.9928
				σ_κ	0.6166	0.7032	0.7108	0.6180	0.4731	0.6349	0.6508
1.932100	1.932450	M2	2	A	302.7962	382.0476	302.3371	328.4834	333.3330	314.9673	321.7252
				δ	**1.18714**	**1.18039**	**1.18510**	**1.18706**	**1.18346**	**1.18702**	**1.18549**
				σ_δ	0.00002	0.00002	0.00002	0.00002	0.00001	0.00002	0.00002
				κ	2.4342	1.2541	1.5842	2.1539	1.0835	2.3502	1.4295
				σ_κ	0.0008	0.0009	0.0009	0.0008	0.0006	0.0008	0.0009
1.932451	1.933500	255.655	3	A	0.8595	0.9835	0.8587	0.9052	0.9133	0.8818	0.8937
				δ	**1.06395**	**1.06653**	**1.07921**	**1.07504**	**1.07460**	**1.06502**	**1.13313**
				σ_δ	0.00515	0.00640	0.00585	0.00538	0.00417	0.00486	0.00622
				κ	–0.1498	1.4082	–0.5542	0.1759	0.2537	0.3255	–0.2973
				σ_κ	0.2773	0.3438	0.3106	0.2867	0.2222	0.2617	0.3146
1.933501	1.936152	MB2	2	A	0.9166	1.1566	0.9152	0.9944	1.0092	0.9534	0.9739
				δ	**1.27831**	**1.23396**	**1.24344**	**1.25110**	**1.22465**	**1.27230**	**1.23437**
				σ_δ	0.00514	0.00574	0.00604	0.00525	0.00395	0.00508	0.00607
				κ	1.4053	0.7005	1.0363	1.0833	0.5380	1.4461	0.9432
				σ_κ	0.2302	0.2663	0.2785	0.2406	0.1850	0.2287	0.2819

Table 3. Amplitude and phase of the annual cycles adjusted to the M2 tidal parameters obtained from analysing successive 3-months periods, sorted as a function of the distance to the Atlantic Ocean. The modulation amplitude estimated by applying eq. (A1) on basis of the observed amplitude factors for the MA2 and MB2 tidal constituents (Table 2) is also presented as well as M2 ocean load amplitude (TPXO.7.2 ocean tide model).

	Annual cycle of the tidal amplitude factor δ		Annual cycle of the tidal phase κ		Modulation amplitude estimate	M2 load amp.	Distance to Atlantic Ocean
	Cycle amplitude	Cycle phase (°)	Cycle amplitude (°)	Cycle phase (°)	$\bar{\delta}_{\mathrm{mod}}$ (eq. A1)	(nms^{-2})	(km)
MB	0.00026	54.027	0.018	3.690	0.00033	16.99	290
WA	0.00020	37.446	0.010	7.093	0.00032	17.72	330
ST	0.00020	29.084	0.014	6.879	0.00026	16.70	470
MO	0.00018	30.274	0.012	17.371	0.00021	12.12	680
WE	0.00018	16.739	0.011	14.442	0.00017	11.98	810
PE	0.00015	24.774	0.007	23.677	0.00012	10.65	920
MC	0.00017	33.851	0.010	21.005	0.00018	12.64	980
CO	0.00016	35.568	0.008	18.428	0.00015	10.58	1070
VI	0.00016	35.213	0.007	24.088	0.00014	10.28	1090

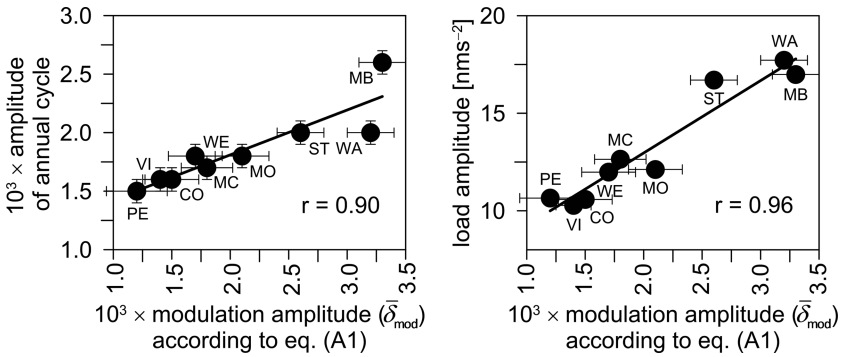

Figure 3. Correlation of the adjusted annual cycle amplitude (left-hand side) and M2 ocean load amplitude (TPXO.7.2 ocean tide model, right-hand side) with the modulation amplitude estimated by applying eq. (A1) at each SG station.

If 1-yr intervals are analysed, the annual modulation cancels out as expected (see also eq. A1). However, other short-term variations, if present, are smoothed out too. Therefore we adjust an annual cycle ($T = 365.25$ d) to the observed M2 tidal parameter at each station and subtract it from the corresponding 3-month time-series to look for short-term features as discussed in the next paragraph. Modulation amplitude and phase of the annual cycles are summarized in Table 3. The amplitude of the M2 annual variation is strongest at MB and WA and gets smaller towards the mid-continental area. The close-by stations CO and VI (60 km apart) show almost the same cycle characteristics. Inserting the anomalous amplitude factors of MA2 and MB2 derived from tidal analysis (Table 2) into eq. (A1) (see Appendix A) allows for estimating the modulation amplitude of the annual cycles. They are added to Table 3 as well as the M2 load amplitude of the TPXO.7.2 ocean tide model and confirm that this modulation is due to anomalous behaviour of MA2/MB2. Note that the adjusted and estimated modulation amplitudes agree fairly well except of the stations closer to the Atlantic Ocean like MB, ST and WA. The correlation between the M2 TPXO.7.2 load amplitude and the estimated modulation amplitude is even stronger as shown in Fig. 3.

Removing the annual modulation of the 3 months analysis

Fig. 4 presents the tidal parameters after subtracting the annual cycles from the 3-month time-series. Common long-term, but sometimes even very short-term features can be clearly identified on both the amplitudes and phases especially at neighbouring stations (e.g. MB–WA–ST, CO–PE–WE). This might be due to common forcing. In 2001 and around 2011, semi-annual modulation is visible coherently appearing at all stations and with similar amplitude at neighbouring stations (e.g. MB–WA–ST around 2011), but does not persist permanently. At MB, it appears with a recurrence period of 4–5 yr. Fig. 4 also displays the air pressure admittances at the SG stations valid in the diurnal and semidiurnal frequency band as adjusted together with the tidal parameters. The seasonal variation reported by Van Dam & Francis (1998) with low values in winter and high values in summer is well pronounced at VI and ST, but less at the others. There is no significant correlation between the temporal variation of admittances and residual amplitude factors or phases. The admittances do not correlate significantly either between the stations, except the pair WA–MB. A possible explanation is that both sites experience atmospheric perturbations approaching from the west in a same manner. The topography met by the meteorological front coming from the ocean is similar, while ST and BH are located in the Rhine valley, which the front meets after weakening on the Belgian Ardennes (and Vosges for ST).

Analysis on 1 year

The common long-term features in the tidal parameter variations are more clearly visible at all SG stations after analysing successive 1-yr intervals (Fig. 5). Similar undulations of the amplitude factors can be observed at almost all stations between 2000.5 and 2007. A relatively sharp decrease of the phase appears from mid 2007 to mid 2008.

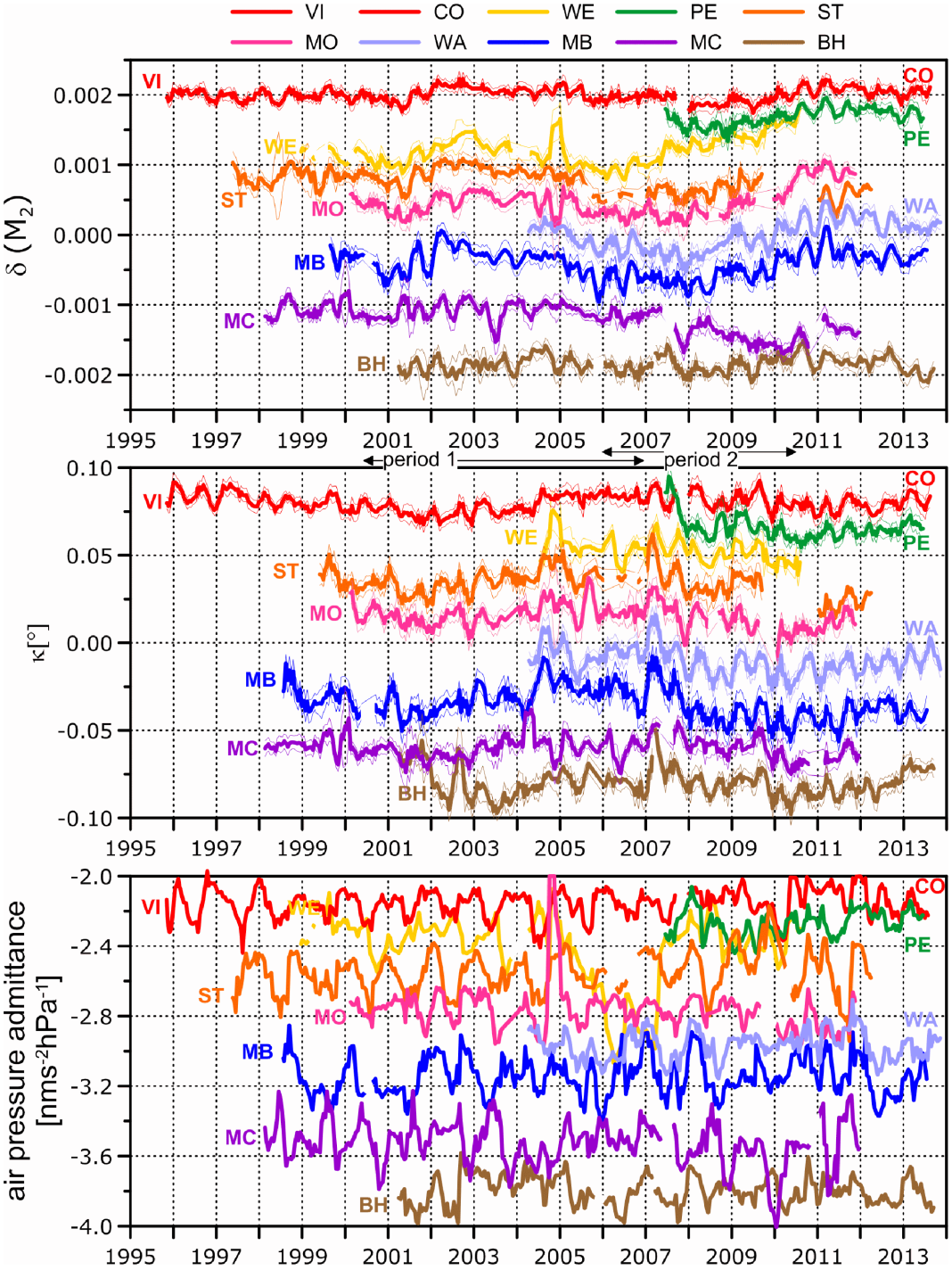

Figure 4. Temporal variation of M2 tidal parameters and air pressure admittance as derived from 3-months gravity time-series after removing the annual cycles (see Table 3). Thin solid lines indicate the errors of the delta factors and phases. At BH a linear trend apparent in the amplitude factors (see Fig. 5) has been removed as well. Arbitrary offsets for clarity reasons. Same offsets for VI and CO.

Fig. 5 also presents the air pressure admittances at the SG stations. Neighbouring SGs at low altitude (MB, WA, ST and BH) show a fairly good correlation, at least during limited periods. This is especially convincing for MB–WA. For sites at higher altitude (e.g. WE, PE and CO) the correlation is weak even if station distances are moderate suggesting topographic effects to play an important role.

Because the single admittance concept is simplifying the real air pressure effect, we also analyse the data after *a priori* correction of the atmospheric effect on gravity based on global load calculations provided by the loading service at the University of Strasbourg (http://loading.u-strasbg.fr/GGP/). It includes atmospheric and induced oceanic loading and makes use of the ECMWF reanalysis (ERA interim) surface air pressure, assuming a barotropic ocean model forced by air pressure and winds (MOG2D, Carrère & Lyard 2003). We select the 6 h resolution model as longer time-series are available than for the 3 h resolution data set. The scatter of the temporal variations at all stations increases strongly.

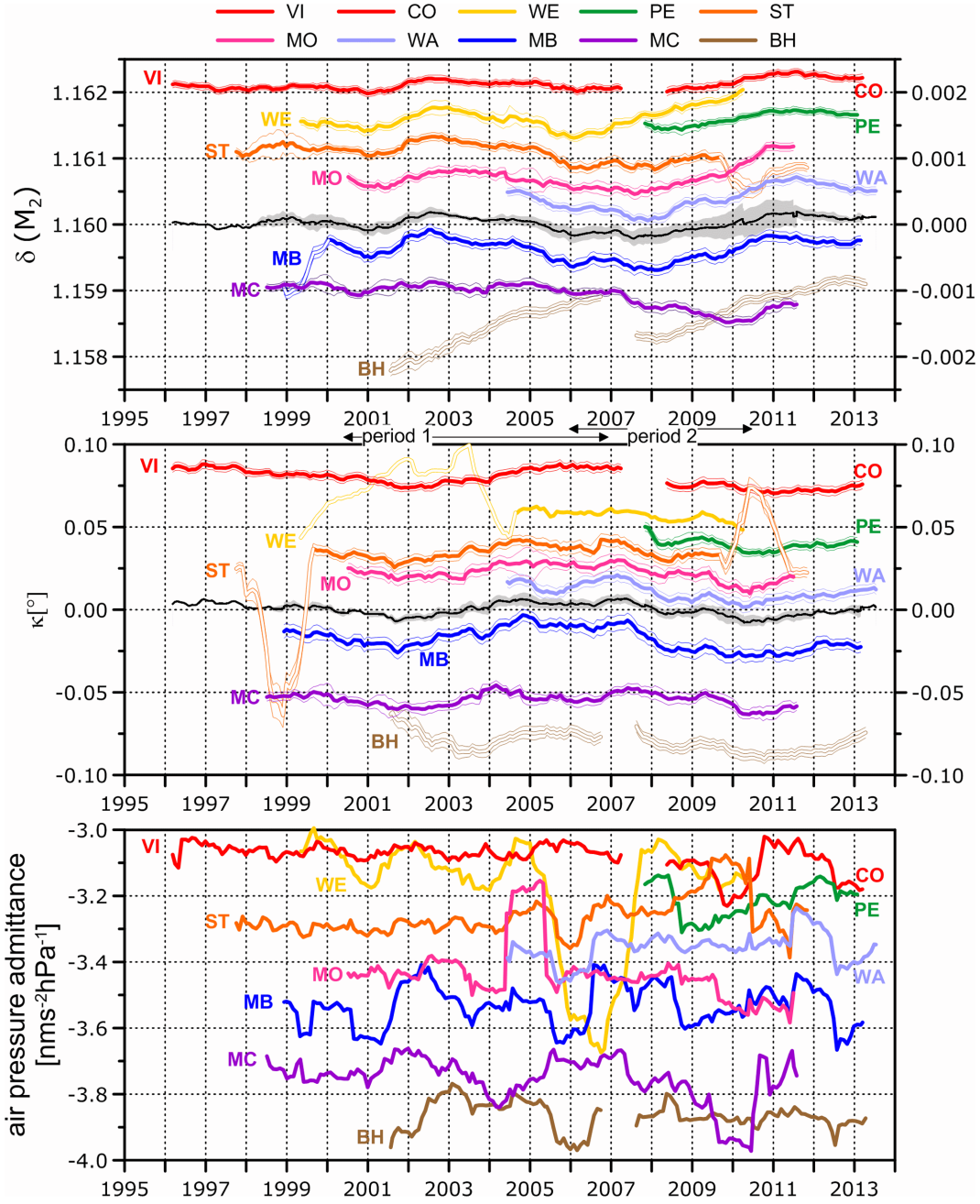

Figure 5. Temporal variation of M2 tidal parameters and air pressure admittance as derived from 1-yr gravity time-series. Thin solid lines indicate the errors of the delta factors and phases. Arbitrary offsets for clarity reasons. Same offsets for VI and CO. Stack results are displayed as black line, standard deviation range as shaded area. White lines mark data disregarded both in correlation analyses and in stacking.

This is probably due to the insufficient correction of local air pressure effects by the global models. However, the main long-term features persist, and the stacking process reveals very similar variations as for the evaluation based on the single admittance concept (Fig. 6). Therefore, we can exclude that atmospheric effects are responsible for the observed temporal variation of tidal parameter.

The variations of the amplitude factor are of the order of ±0.2‰. This number sets (1) an upper accuracy limit for earth tide model validation based on 1-yr observation periods assuming perfectly calibrated gravimeters and perfect ocean models and (2) estimates the stability level of SG scale factors.

We can only speculate why Calvo *et al.* (2014) did not reveal common features in the M2 tidal parameter variations although they applied 1-yr analyses on most of our SG time-series as well. We suspect that their time-series were noisier as only one has been pre-processed by station operators. Only the latter have best knowledge of instrumentally induced distortions, offsets etc. deteriorating the frequency spectrum and are able to correct for them in an optimal way. For example, fig. 13 of Calvo *et al.* (2014) presents the temporal M2 variations for VI in detail. However, they do not match our findings at all. In our investigation, ST and WE, for example, reveal distortions in the time-series (see Fig. 5) that possibly would disappear if we had analysed data provided by the station operators.

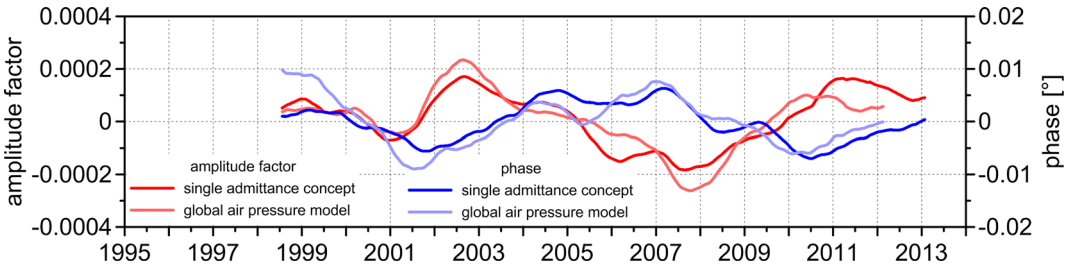

Figure 6. Stacked M2 tidal parameters obtained by different consideration of atmospheric load effects: adjustment of a constant air pressure admittance factor by tidal analysis (dark red and dark blue) versus subtraction of atmospheric load effects [MOG2D model, Carrère & Lyard (2003), http://loading.u-strasbg.fr/GGP/] before tidal analysis (light red and light blue).

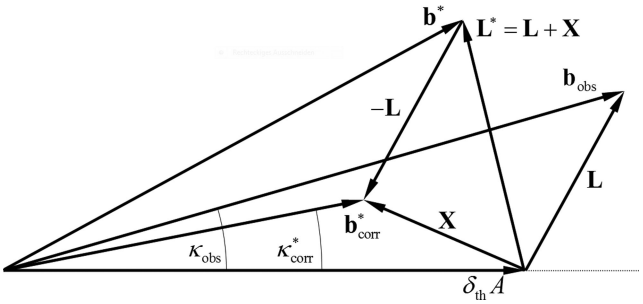

Figure 7. Vector diagram of tide and ocean loading vectors. Tidal vectors: $\mathbf{b}_{obs}$ observed in case of un-perturbed load vector $\mathbf{L}$, $\mathbf{b}^*$ observed in case of perturbed load vector $\mathbf{L}^*$, $\mathbf{b}^*_{corr}$ observed in case of perturbed load vector $\mathbf{L}^*$ corrected for unperturbed load vector $\mathbf{L}$, $\mathbf{X}$ residual vector.

Fig. 5 confirms the calibration results achieved for the SG operating at VI and CO regarding both scale factor and time lag. Note that the arbitrary offset chosen for VI and CO in Figs 4 and 5 is identical for both stations. Considering the small spatial separation (60 km), we may assume the load correction to be accurate or at least to exhibit the same errors at both stations. Therefore, considering both time-series as only one makes sense: the VI and CO time-series follow almost perfectly the average variations (stack) seen at the other SG sites. Fig. 5 also shows obvious trends for the SG at BH of unknown origin and problems with the time lag at ST and WE. This proves comparing the temporal tidal parameter variations to be a valuable tool for detecting calibration problems (scale factor or time lag).

Correspondence to temporal load vector variations

The observed tidal parameter variation can be formally translated into equivalent temporal changes of the load vector. Suppose A to be the amplitude of a specific tidal constituent, $\mathbf{L}$ the load vector predicted by the ocean load model, and δ_{th} the theoretical amplitude factor. Assuming that the ocean model is correct and observed gravity is error-free, the observed tidal vector $\mathbf{b}_{obs}$ can be decomposed into its in-phase and out-of-phase components (Fig. 7):

$$\mathbf{b}_{obs} = (\delta_{th} A + L_i, L_o),$$

where L_i, L_o denote the in-phase and out-of-phase components of the load vector, respectively. The relation to observed tidal parameters $\delta_{obs}, \kappa_{obs}$ is given by

$$\delta_{obs} = \frac{|\mathbf{b}_{obs}|}{A} \qquad \kappa_{obs} = \text{atan}\left(\frac{L_o}{\delta_{th} A + L_i}\right).$$

If one can perfectly correct for ocean load $\mathbf{L}$, the corrected tidal vector $\mathbf{b}_{corr}$ and amplitude factor δ_{corr} read as

$$\mathbf{b}_{corr} = (\delta_{th} A, 0)$$
$$\delta_{corr} = \delta_{th}$$

corresponding to the body tide model with the residual vector $\mathbf{X}$ being the zero vector in this ideal case.

In case of a perturbed load vector $\mathbf{L}^* = (L_i + \Delta L_i, L_o + \Delta L_o)$ the in-phase and out-of-phase perturbations ΔL_i, ΔL_o are directly linked just to the residual vector $\mathbf{X}$. The observed tidal vector $\mathbf{b}^*$, the corrected tidal vector $\mathbf{b}^*_{corr}$ and corrected tidal parameters δ^*_{corr}, κ^*_{corr} now read as:

$$\mathbf{b}^* = (\delta_{th} A + L_i + \Delta L_i, L_o + \Delta L_o)$$

$$\mathbf{b}^*_{corr} = \mathbf{b}^* - \mathbf{L} = [\delta_{th} A + \Delta L_i, \Delta L_o] = \mathbf{b}_{corr} + \mathbf{X}$$

$$\delta^*_{corr} = \frac{1}{A}\sqrt{(\delta_{th} A)^2 + 2\delta_{th} A \Delta L_i + (\Delta L_i)^2 + (\Delta L_o)^2}$$

$$\kappa^*_{corr} = \text{atan}\left[\frac{\Delta L_o}{\delta_{th} A + \Delta L_i}\right].$$

The results for MB and ST based on the TPXO7.2 model (Egbert & Erofeeva 2002) are displayed in Fig. 8. The path of the load vector perturbation (ΔL_i, ΔL_o) is similar at both sites and indicates a loop lasting over 8–9 yr. It is worth mentioning again that 3rd degree tidal constituents close to the main M2 wave (Fig. 1) are able to modulate M2 with this period. An explanation for the observed variation of tidal parameters could be time varying M2 load. The perturbations ΔL_i, ΔL_o would need to vary by less than $\pm$ 0.1 nms^{-2} at MB and ST corresponding to 1‰ of the load approximately. At VI (not shown here), it is even smaller ($\pm$0.05 nms^{-2}) due to the larger distance to the Atlantic Ocean. This is consistent to the M2 amplitude factors, which are similar at MB and ST, but much lower at VI than at MB (see Table 2). Although variable loading may play a role, this could only be tested when time-series longer than 18.6 yr are available. Meanwhile, our preferred explanation is a dominating effect due to the 3rd degree tidal constituents close to the main M2 wave (Fig. 1) which are able to modulate M2 with this period. This hypothesis is tested in Section 4.

3 CORRELATION ANALYSIS OF THE 12-MONTH TIME-SERIES

First, we identify periods showing common features by stacking all tidal parameter time-series and evaluating the RMS deviation from the stacking result (black lines in Fig. 5). As BH obviously

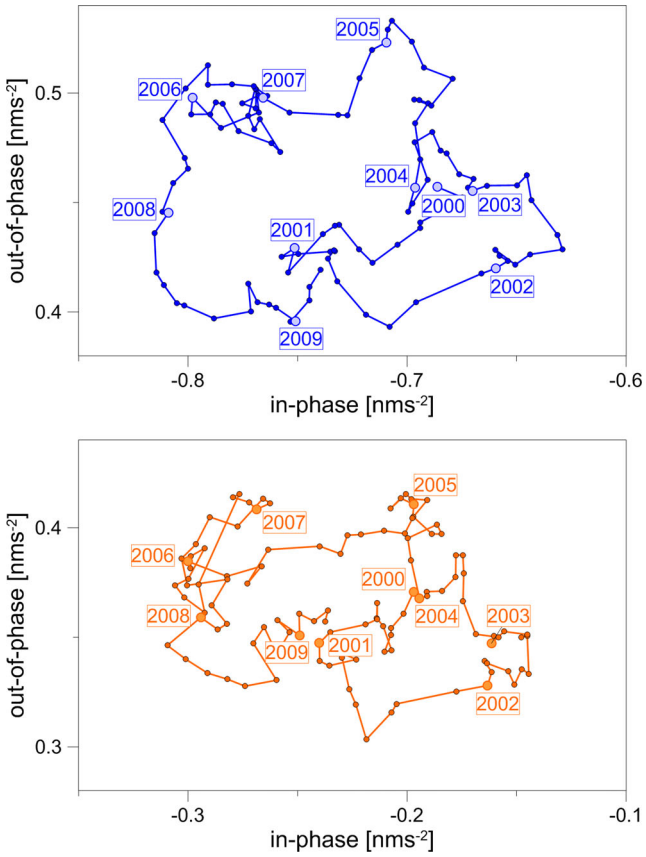

Figure 8. Path of the in-phase and out-of-phase components ΔL_i, ΔL_o of the load vector perturbation (dotted line) at MB (top panel) and ST (bottom panel). Numbers reflect the year of the observation epoch (1-yr intervals shifted in steps of 1 month).

experiences an apparent change in its scale factor, this station is not considered for stacking. Few other time-series (e.g. ST, WE) sometimes show obvious distortions either in the amplitude factor or in the phase presumably due to SG calibration or instrumental problems. These parts are excluded as well. We identify two time periods during which the stacked tidal parameter variation (black lines in Fig. 5) exceeds its rms (shaded areas in Fig. 5): 2000.5–2007 and 2006–2010.5. Obviously, the modulation is stronger at that time. Then we calculate the correlation coefficients between the M2 tidal parameters of all station pairs using data within the two selected periods only (1) and within the entire time-series (2) (Table 4). Note that the correlation study makes sense only as long as the time-series of station pairs overlap sufficiently. Again, we do not consider BH and a few distorted parts in other time-series.

We first calculate the correlation coefficient and then determine the probability that the null hypothesis of zero correlation has to be rejected. In the period between 2000.5 and 2007 positive correlation is found in 18 of 21 station pairs (86 per cent) for the amplitude factors while between 2006 and 2010.5 positive correlation is found in 16 of 20 station pairs (80 per cent) for the phases. For the complete time-series, a positive correlation >0.7 (coefficient of determination >0.5) is observed in 18 of 31 cases (58 per cent) for the amplitude factor and in 20 of 31 cases (65 per cent) for the phase variation. In general, MC shows the poorest fit than any other station, which is also visible in Fig. 5. This might reflect Adriatic Sea effects to be less prominent at the other sites or Atlantic Ocean effects to be less prominent at MC. Disregarding MC thus increases the percentage of positive correlations of the whole time-series to 72 per cent (amplitude factor and phase). These statistically significant variations are due to the frequency resolution problem in tidal analysis and/or reflect a possible common forcing.

The correlation is stronger for the stations closer to the Atlantic Ocean (MB, WA and ST). To assess this quantitatively, we adjust a linear fit to the relation between the tidal parameter variation at each station and the stacking result. Fig. 9 plots the regression coefficients as a function of the minimum distance to the Atlantic Sea and North Sea/Baltic Sea, respectively. The regression coefficient increases clearly with decreasing distance to the Seacoast. For the 3-month analyses, this is even more pronounced as the annual modulation amplitude dominates over the long-term variations, but it makes the correlation analysis questionable (Van Camp *et al.* 2014). Interestingly, the same tendency exists for the annual cycle amplitude of the parameter based on 3-month tidal analyses (Table 3). The amplitude of both the annual and the long-term M2 modulation are stronger at stations closer to the Atlantic Sea because the amplitude of the ocean load vector increases with decreasing distance to the sea (see also Fig. 2).

4 FREQUENCY RESOLUTION PROBLEM OF TIDAL ANALYSIS

As stated on point (3) of Section 1, temporal variations can be due to numerical artefacts. In tidal analyses we need to combine constituents into groups assuming equal tidal parameters within a group. However, this basic assumption is violated due to implicitly mixing constituents

(1) with degree and order dependent response to elastic tidal deformation
(2) and/or with different response to ocean load.

Modern tidal prediction and analysis codes like ETERNA (Wenzel 1996) or ET34-ANA-V50 (Schüller 2015) consider the *a priori* response of the Earth to constituents of different degree and order, derived from global solid, elastic Earth tide models. In addition, ET34-ANA-V50 (Schüller 2015) allows for collecting constituents of different degree and order in specific sub-groups provided the time-series is sufficiently long. ETERNA (Wenzel 1996) makes use of the Wahr–Dehant–Zschau (WDZ) body tide model (Dehant 1987). However, it does not consider different response to loading, if present. Unfortunately, it is impossible to assess the loading effects directly, because no ocean load models exist for 3rd degree tidal waves. In Europe, observed 2nd degree M2 amplitude factors typically increase due to ocean loading by about 2.3 per cent with respect to those predicted by the Dehant–Defraigne–Wahr (DDW) body tide model (Dehant *et al.* 1999).

Ducarme (2012) investigated main lunar waves generated by the third degree tidal potential. He analysed long SG gravity time-series and found that the mean values of the 3rd degree waves 3MK2 and 3MO2 within the semi-diurnal frequency band are 0.3 per cent lower than those predicted by the DDW body tide model (Dehant *et al.* 1999). This differs significantly from the 2.3 per cent experienced by the 2nd degree waves. Hence, as long as the time-series is not long enough to separate the 2nd and 3rd degree waves, the 3rd degree constituents as shown in Fig. 1 are expected to cause the M2 modulation. This is the case too for the 2nd degree waves but the effect is much reduced when using 1-yr series, as explained in Section 2.

Therefore, we investigate here the frequency resolution problem by analysing synthetic time-series at MB, ST and VI. We calculated

Table 4. Correlation of the temporal tidal parameter variation (M2). Bold letters indicate significant (>95 per cent level) positive correlation coefficients >0.7. The significance level (rounded, in [per cent]) is given in parentheses.

Period 2000.5–2007, amplitude factor: positive correlation >0.7 is found in 18 of 21 pairs (86 per cent) for the amplitude factors

	MB	MC	MO	ST	VI	WA
MC	**0.71(100)**					
MO	**0.85(100)**	0.51(100)				
ST	**0.96(100)**	0.69(100)	**0.87(100)**			
VI	**0.82(100)**	**0.70(100)**	**0.80(100)**	**0.78(100)**		
WA	**0.95(100)**	**0.92(100)**	**0.89(100)**	**0.89(100)**	**0.88(100)**	
WE	**0.93(100)**	0.66(100)	**0.83(100)**	**0.91(100)**	**0.85(100)**	**0.74(100)**

Period 2000.5–2007, phase

	MB	MC	MO	ST	VI	WA
MC	0.68(100)					
MO	**0.83(100)**	**0.75(100)**				
ST	**0.93(100)**	**0.79(100)**	**0.89(100)**			
VI	**0.84(100)**	0.54(100)	**0.87(100)**	**0.82(100)**		
WA	0.22(81)	0.47(100)	0.10(044)	0.44(99)	–0.32(94)	
WE	0.53(100)	0.11(47)	0.36(97)	0.45(99)	–0.28(89)	0.10(43)

Period 2006–2010.5, amplitude factor

	MB	MC	MO	PE	ST	WA
MC	–0.51(100)					
MO	**0.88(100)**	–0.78(100)				
PE	**0.75(100)**	–0.89(100)	**0.85(100)**			
ST	**0.75(100)**	–0.56(100)	**0.78(100)**			
WA	**0.94(100)**	–0.53(100)	**0.89(100)**	0.64(100)	**0.70(100)**	
WE	0.58(100)	–0.95(100)	**0.80(100)**	**0.84(100)**	**0.71(100)**	0.56(100)

Period 2006–2010.5, phase: positive correlation >0.7 is found in 16 of 20 pairs (80 per cent) for the phases

	MB	MC	MO	PE	ST	WA
MC	0.48(100)					
MO	**0.89(100)**	0.61(100)				
PE	**0.83(100)**	**0.79(100)**	**0.72(100)**			
ST	**0.85(100)**	0.21(084)	**0.89(100)**			
WA	**0.97(100)**	0.55(100)	**0.88(100)**	**0.88(100)**	**0.89(100)**	
WE	**0.84(100)**	**0.72(100)**	**0.87(100)**	**0.83(100)**	**0.81(100)**	**0.88(100)**

All data, amplitude factor: positive correlation >0.7 is found in 18 of 25 pairs (72 per cent) for the amplitude factors (without data from MC)

	CO	MB	MC	MO	PE	ST	VI	WA
MB	**0.96(100)**							
MC	0.22(082)	0.27(100)						
MO	**0.98(100)**	**0.74(100)**	–0.29(100)					
PE	**0.97(100)**	**0.94(100)**	0.03(018)	**0.97(100)**				
ST		**0.96(100)**	0.64(100)	**0.85(100)**				
VI		**0.76(100)**	0.57(100)	**0.80(100)**		0.69(100)		
WA	**0.97(100)**	**0.97(100)**	–0.14(080)	**0.90(100)**	**0.93(100)**	**0.87(100)**	**0.88(100)**	
WE		0.27(100)	–0.59(100)	0.63(100)	**0.84(100)**	0.37(100)	**0.84(100)**	0.32(099)

All data, phase: positive correlation >0.7 is found in 18 of 25 pairs (72 per cent) for the phases (without data from MC)

	CO	MB	MC	MO	PE	ST	VI	WA
MB	0.14(071)							
MC	**0.83(100)**	0.62(100)						
MO	0.34(097)	**0.87(100)**	**0.71(100)**					
PE	0.69(100)	**0.71(100)**	**0.89(100)**	**0.78(100)**				
ST		**0.88(100)**	0.62(100)	**0.89(100)**				
VI		**0.83(100)**	0.53(100)	**0.87(100)**		**0.82(100)**		
WA	0.16(078)	**0.89(100)**	0.66(100)	**0.85(100)**	**0.70(100)**	**0.79(100)**	–0.32(094)	
WE		**0.86(100)**	0.58(100)	**0.87(100)**	**0.83(100)**	**0.82(100)**	–0.28(089)	**0.81(100)**

DDW body tides predicted by ETERNA (Wenzel 1996) using the tidal potential catalogue by Hartmann & Wenzel (1995a) and added ocean load tides by applying the SPOTL package (Agnew 2012) based on the TPXO7.2 model. SPOTL uses loads for a smaller number of constituents and a smoothed admittance to compute a time series considering 342 constituents of the CTE tidal potential catalogue by Cartwright & Taylor (1971) and Cartwright & Edden (1973). SPOTL does not include any 3rd degree tidal constituent, that is there is no loading for those waves in the synthetic time-series.

In Table 5 we compare tidal analyses of observed and synthetic time-series at MB, ST and VI. The analysis separates the waves MA2 and MB2 within the M2 group, which are able to cause the annual modulation. Two 3rd degree wave groups (255.455 and 255.655) are also evidenced that contain constituents potentially causing the 8.85 yr modulation. The amplitude factors of the waves 255.455

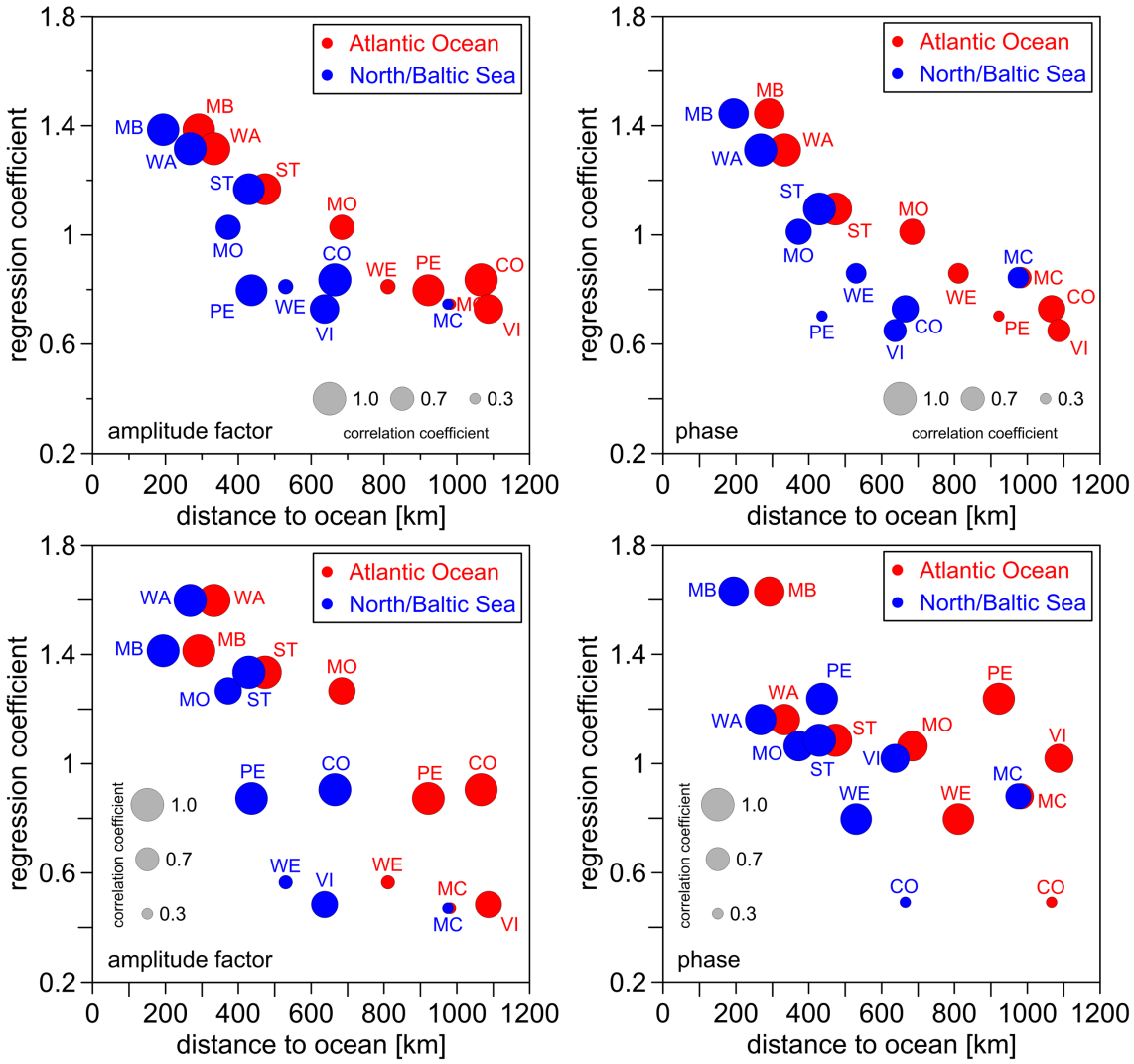

Figure 9. Regression coefficient obtained by fitting a linear relation between M2 tidal parameter variation and stacking result: 3 month time-series (upper panel), 1-yr time-series (lower panel). Circle size reflects the magnitude of the correlation coefficient as shown by the grey bubbles.

and 255.655 reported in Table 5 are close to the DDW body tide model prediction. The same holds true, within the error bars, for all stations with time-series long enough for applying this wave group separation (see Table 2). The amplitude factors of the 255.455 and 255.655 frequency bands next to M2 are similar almost everywhere. In order to check if the result is independent from the grouping, we also used the analysis code ET34-ANA-V50 by Schüller (2015) and collected higher potential degree constituents in subgroups: M2#3 contains all 3rd degree constituents within the M2 group, V31 and V32 those of order 1 and 2, respectively in all other diurnal and semi-diurnal groups (Table 5). The M2#3 amplitude factors match the DDW body tide model closely as well as the 3rd degree waves do within V31 and V32, except of ST which is probably due to the amplitude factor and phase distortion observed there. This proves that 3rd degree waves experience less ocean loading than 2nd degree components and agrees with the result obtained by Ducarme (2012) for the semi-diurnal wave groups 3MK2 and 3MO2 showing them comparable to O1 (less loading).

Note, that according to the Rayleigh criterion the observed time-series are not long enough to separate 255.455 and 255.655 from M2. However, especially in least squares adjustment, the Rayleigh-criterion is by far too pessimistic (Schüller 2015). The analysis codes ETERNA (Wenzel 1996) and ET34-ANA-V50 (Schüller 2015) report the condition number as a criterion for numerical stability regarding the resolution. Based on the provided condition numbers the analysis result can be regarded as reliable.

Thus the requirement that all waves within the group have equal tidal parameters is not met, that is the assumption of tidal parameters being equal for all constituents within the M2 group is wrong, given that the 3rd degree constituents are not as influenced by the ocean loading effects as the 2nd degree waves. This causes M2 modulation effects when the waves cannot be separated from the M2 group as it is the case for 1-yr analyses. At least 18-yr analyses would be needed to suppress the modulation.

We perform consecutive tidal analyses of 1-yr data windows shifted over the synthetic time-series and compare the results with those of the observed data at MB, ST and VI (Fig. 10). The M2 amplitude factors of the synthetic time-series (Fig. 10, light dashed lines) reflect the same long-term (roughly 9-yr) modulation as those of the observed ones (Fig. 10, dark solid lines) at all stations. At ST, irregularities in the phase and in the amplitude factor are visible around the beginning and the end (see also Fig. 5). Here, the temporal tidal parameter variations of the synthetic tides (Fig. 10, light orange dashed line) do not match those of the observed

Table 5. Tidal analysis results for the synthetic tides and observed data for MB, ST and VI. Synthetic time-series: DDWi body tides + ocean load based on the TPXO7.2 model, calculated by SPOTL (Agnew 2012). Last two columns indicate degree and order of the largest wave within a group.

			ETERNAv3.4				ET34-ANA-V50			
		Ampl.	Synthetic time-series (36 yr)		Observed time-series					
		(nms^{-2})	δ	κ (°)	δ	κ (°)	δ	κ (°)	d	o
MA2	MB	1.0409	1.18805 ± .00007	2.4675 ± .0032	1.21412 ± .00454	1.0620 ± .2140	1.21486 ± .00393	1.035 ± .186	2	2
	ST	1.1293	1.18856 ± .00006	2.2050 ± .0030	1.21558 ± .00461	0.3870 ± .2174	1.21329 ± .00529	1.705 ± .250		
	VI	1.1459	1.18356 ± .00004	1.1000 ± .0019	1.19092 ± .00351	–0.3569 ± .1690	1.19106 ± .00331	–0.342 ± .159		
255.455	MB	0.3229	1.07205 ± .00016	1.0165 ± .0087	1.07427 ± .01156	0.0299 ± .6166			3	2
	ST	0.3400	1.07335 ± .00015	0.9717 ± .0081	1.07813 ± .01163	1.1248 ± .6180				
	VI	0.3431	1.07745 ± .00010	0.5911 ± .0053	1.07542 ± .00888	1.5397 ± .4731				
M2	MB	302.7956	1.18879 ± .00000	2.4046 ± .0000	1.18714 ± .00002	2.4342 ± .0008	1.18712 ± .00002	2.434 ± .001	2	2
	ST	328.4828	1.18918 ± .00000	2.1451 ± .0000	1.18706 ± .00002	2.1539 ± .0008	1.18700 ± .00002	2.148 ± .001		
	VI	333.3324	1.18379 ± .00000	1.0651 ± .0000	1.18346 ± .00001	1.0835 ± .0006	1.18347 ± .00001	1.084 ± .001		
255.655	MB	0.8596	1.07829 ± .00008	0.1114 ± .0042	1.06395 ± .00515	–0.1498 ± .2773			3	2
	ST	0.9053	1.07817 ± .00007	0.1050 ± .0039	1.07504 ± .00538	0.1759 ± .2867				
	VI	0.9133	1.07793 ± .00005	0.0521 ± .0026	1.07460 ± .00417	0.2537 ± .2222				
MB2	MB	0.9171	1.18926 ± .00008	2.3017 ± .0037	1.27831 ± .00514	1.4053 ± .2302	1.27879 ± .00447	1.448 ± .200	2	2
	ST	0.9949	1.18951 ± .00007	2.0496 ± .0033	1.25110 ± .00525	1.0833 ± .2406	1.25674 ± .00602	–0.118 ± .274		
	VI	1.0096	1.18379 ± .00005	1.0127 ± .0022	1.22465 ± .00395	0.5380 ± .1850	1.22485 ± .00373	0.519 ± .175		
M2#3	MB	0.8595					1.06286 ± .00436	–0.395 ± .235	3	2
	ST	0.9052					1.14173 ± .00591	1.435 ± .297		
	VI	0.9132					1.07261 ± .00381	0.306 ± .203		
V31	MB	2.7279					1.07723 ± .00323	0.517 ± .172	3	1
	ST	2.5951					1.07774 ± .00317	0.695 ± .169		
	VI	2.5674					1.07303 ± .00281	0.512 ± .150		
V32	MB	5.7014					1.06569 ± .00066	0.192 ± .036	3	2
	ST	6.0045					1.06757 ± .00093	0.071 ± .050		
	VI	6.0580					1.07008 ± .00060	0.123 ± .032		

time-series (Fig. 10, orange solid line). Contrarily, the fit is almost perfect (Fig. 10, red solid resp. light red dashed line) at VI, where only little distortions are present. Note also the almost perfect fit to the observed data at CO (especially for the amplitude factor) which again confirms the SG GWR C025 scale factor derived from calibration experiments at VI and CO (Meurers 2012) to be accurate on the level of a few 0.1‰.

These findings suggest that the temporal tidal parameter variations seen in the observed 1-yr time-series are most likely due to the frequency resolution problem induced by degree dependent response to ocean loading. However, because the modulation amplitudes are as small as 0.2‰, they are detectable only in high quality gravity data.

In a second step, we first subtract the 3rd degree DDW body tides from the observed time-series at MB, ST and VI and then analyse consecutive 1-yr intervals (Fig. 10, dark dashed lines). As expected, the 9-yr modulation disappears but the short-term modulations remain and show common features again. These modulations are probably caused by inseparable 2nd degree waves within the M2 group. If they could be separated from each other (as in extremely long time-series), they are expected to be associated with anomalous tidal parameters different from the main M2, similarly as it is the case for the MA2 and MB2 waves (Tables 2 and 5). Thus they are interpretable as temporal M2 load variation.

Accuracy limit of tidal parameter determination

Finally, we investigate the accuracy limit of tidal parameter determination due to the modulation effect as a function of the length of the analysis interval. For that purpose, we use synthetic tides at MB and analyse windows of increasing length shifted over the entire time-series in steps of 3 months. As expected, the scatter of M2 amplitude factors decreases with the interval length (Fig. 11) due to the time integration effect (see Appendix A). The envelope provides an estimate of the accuracy limit. Assuming a perfectly calibrated SG, the error due to the modulation effect is always smaller than about 0.3‰ even for intervals as short as 1 yr. The error never exceeds 0.1‰ for intervals equal or longer than 8 yr. A M2 phase bias of 0.005° w.r.t. body tide models cannot be interpreted reliably if the interval length is smaller than 7 yr. On the other hand, amplitude factors derived from 3-month intervals may be biased by up to 0.6‰. These results of course depend on the SG site because stronger ocean loading may increase the modulation effect as shown in Table 3. They also set an upper accuracy limit for the scale factor determination of relative gravimeters if the latter are calibrated against a synthetic tide model (given it is perfect). If the calibration is done in the spectral domain, the resulting scale factor may be biased due to the M2 modulation.

5 SUMMARY AND CONCLUSIONS

We revealed common features in the temporal variation of M2 tidal parameters derived from 10 European SG gravity time-series. This was done by tidal analysis of successive 3-months and 1-yr intervals and shifting the analysis window over each SG time-series.

For the 3-months analyses, we adjusted annual cycles to the M2 modulation caused by the anomalous tidal parameters of the MA2, MB2 constituents. The modulation amplitudes agree fairly well with estimates based on the MA2, MB2 amplitude factors inferred from long (>1 yr) gravity time-series. They tend to increase with

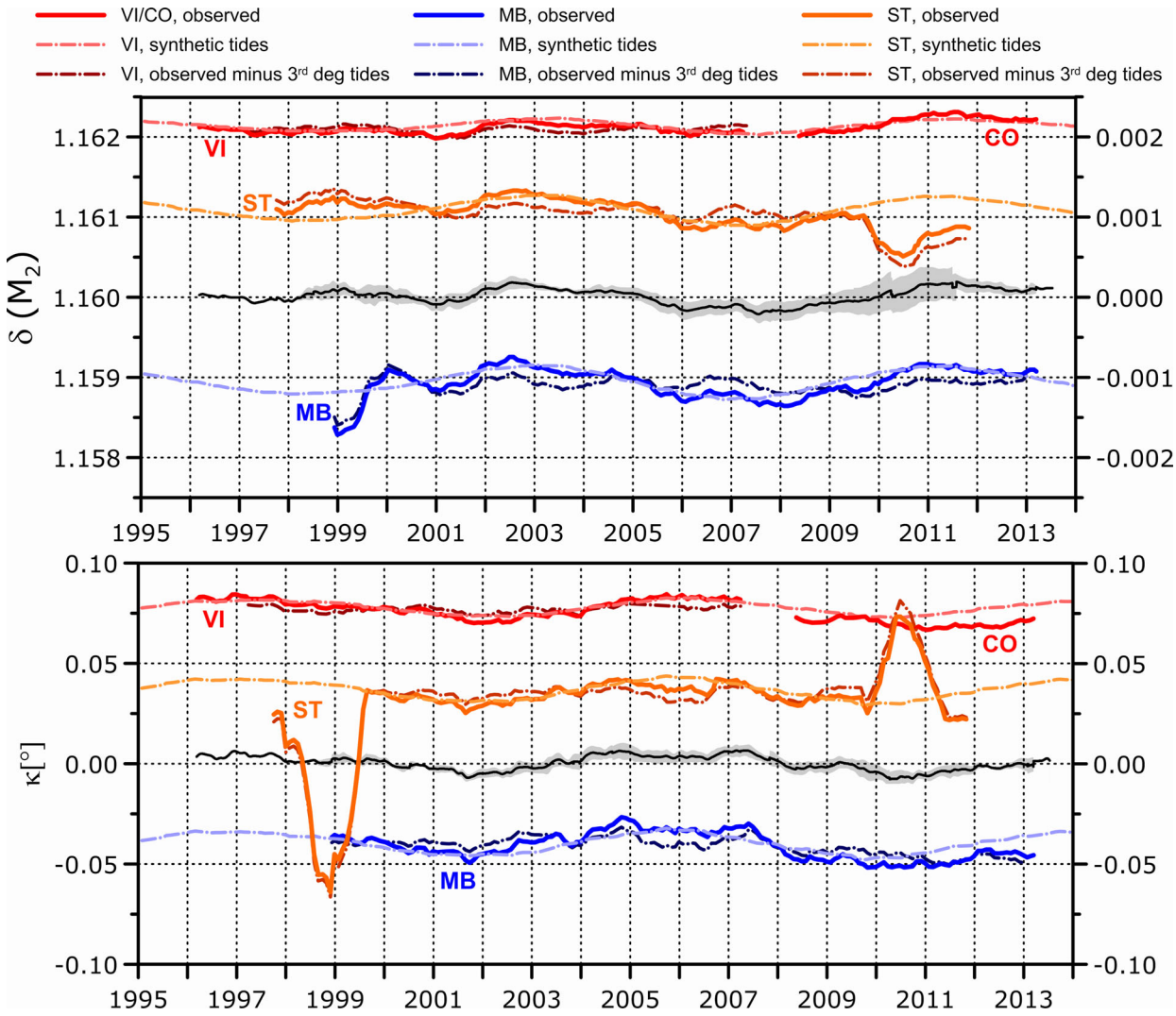

Figure 10. Temporal variation of tidal parameters as provided from the analyses of synthetic tide models and observed data at MB, ST and VI. Observed: bold solid lines. Synthetic time-series (DDW body tides + TPXO7.2 ocean load): dashed lines, light colours. Observed minus 3rd degree DDW body tides: dashed lines, dark colours. For comparison, stack results and their standard deviation range already shown in Fig. 5 are displayed again by the black line and the shaded area.

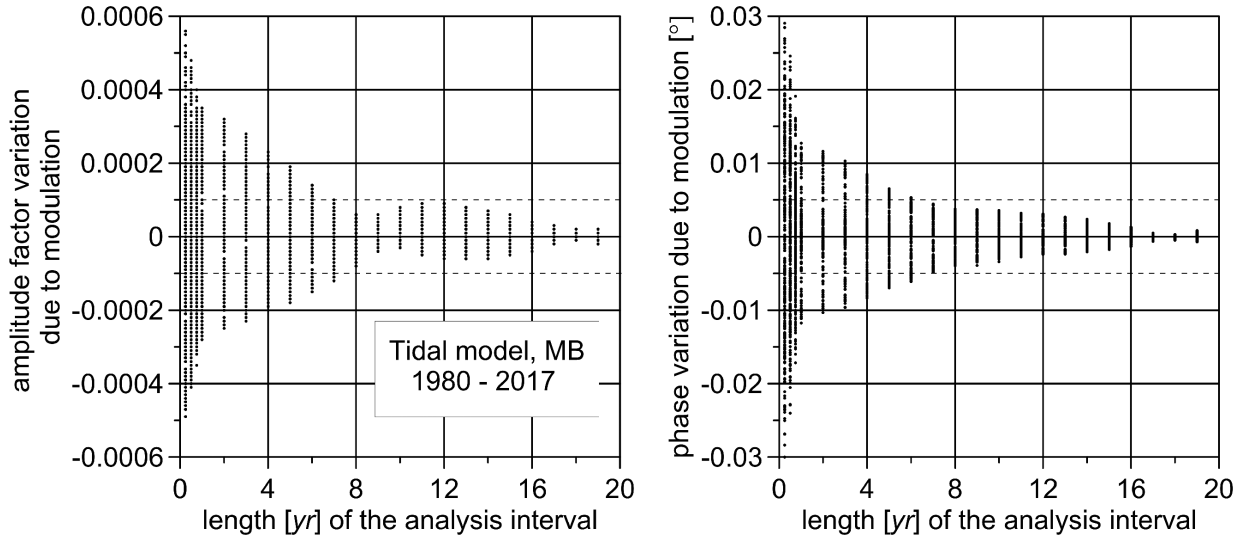

Figure 11. Scatter of M2 tidal parameters at MB station derived from tidal analyses of windows with increasing length shifted over the entire time-series by steps of 3 months.

decreasing distance of the stations to the Atlantic Ocean. After removing the annual cycles, common interannual variations appear and are traceable especially at neighbouring stations.

For the 1-yr analyses, we identified statistically significant temporal short- and long-term variations of tidal parameters, as large as 0.2‰, by applying a stacking procedure. They turn out to appear coherently at most European SG stations, contrary to the results of Calvo *et al.* (2014). Only Medicina (MC) close to the Adriatic Sea shows a different behaviour. We performed a correlation analysis using all station pairs to assess these findings quantitatively whereby a few distorted portions were excluded. For the complete time-series, a positive and statistically significant (>95 per cent level) correlation of >0.7 is observed in 58 per cent of all pairs for the amplitude factor and 65 per cent for the phase variation. When disregarding the MC station, positive correlation coefficients larger than 0.7 exist for 72 per cent of all station pairs for the amplitude factors and phases. We identified two periods (2000.5–2007 and 2006–2010.5) where the tidal parameter variations exceeded the stack error range, because the modulation due to the poor frequency resolution seems to be stronger at that time. For these selected time periods the correlation is even better (80–86 per cent). The variations get stronger with decreasing distance to the coastline of the Atlantic Ocean.

We applied two analysis procedures for considering the atmospheric effect differently: adjustment of a constant air pressure admittance factor derived from tidal analysis and subtraction of atmospheric load effects (MOG2D model, Carrère & Lyard (2003, http://loading.u-strasbg.fr/GGP/) before tidal analysis. They suggest that the tidal parameter variations are not caused by imperfect models of the atmospheric effects.

The following conclusions can be drawn:

(1) Comparison with synthetic tide models suggests the M2 tidal parameter variation to be caused by insufficient frequency resolution of limited time-series as 2nd and 3rd degree constituents within the M2 group respond differently to ocean loading. Therefore, we expect long-term modulation of the M2 tidal parameter in analyses of consecutive 1-yr intervals. The path of load vector increments equivalent to the temporal changes of tidal parameters reveals the presence of a roughly 9-yr modulation with load vector variations in the order of 1‰. The load vector variations can be represented by M2-satellites with frequencies very close to the M2 frequency, which cannot be separated from M2 in 1-yr analyses. The modulation amplitude is as small as 0.2‰ but we could capture them in the investigated SG time-series. If the scale factor instability were larger, it would be very unlikely to observe common features in the tidal parameter variations of M2. This temporal stability justifies averaging the SG scale factors derived from repeated calibration experiments to increase the scale factor accuracy well below the 1‰ level (Van Camp *et al.* 2016). The amplitude factors for different SGs scatter around the average variation (stack in Fig. 5) with a standard deviation smaller than 0.05‰. Again, there is a clear tendency of increasing modulation amplitude with decreasing distance to the coastline.

(2) We cannot exclude that temporal variations of the ocean load contribute as well. The annual M2 modulation of 3-month analyses certainly reflects such seasonal load variations. However, our time-series are still too short to prove reliably similar effects for the observed long-term modulation of the 1-yr analysis results.

(3) The observed variations impose an upper accuracy limit of about 0.2‰ for body tide model validation even for perfectly calibrated instruments as long as 1-yr time-series are used. The 0.1‰ error is never exceeded for intervals equal or longer than 8 yr. Earth body tide model validation should be based on long time-series being a multiple of 1-yr periods to mitigate the M2 tidal parameter modulation problem.

(4) The calibration of relative gravimeters based on tidal models (provided they are perfect) is limited to slightly less than 1‰ if 3-month periods are evaluated, or to about 0.5‰ for half-year periods.

(5) Finally, the analysis of temporal variations of tidal parameters and their comparison with other stations is an appropriate way to control the quality of the transfer function of the gravimeters and to identify disturbed portions of gravity time-series.

ACKNOWLEDGEMENTS

We thank ICET and the GFZ-ISDC data centre for providing the SG time-series, M.S. Bos and H.G. Scherneck for their ocean loading provider tool, J.P. Boy for providing global load calculations as well as K. Schüller and D.C. Agnew for providing the software codes ET34-ANA-V50 and SPOTL, respectively. We are grateful to all the SG operators for ensuring long term, high quality continuous gravity data, which remains a challenging task. Finally, yet importantly, we thank the editor D.C. Agnew and two anonymous referees for their careful reviews, which were extremely helpful in improving the paper.

REFERENCES

Agnew, D.C., 2012. SPOTL: Some Programs for Ocean-Tide Loading, SIO Technical Report, Scripps Institution of Oceanography, Available at: http://escholarship.org/uc/item/954322pg, last accessed 17 November 2015.

Amin, M., 1985. Temporal variations of tides on the west coast of Great Britain, *Geophys. J. R. astr. Soc.,* **82,** 279–299.

Baker, T.F. & Alcock, G.A., 1983. Time variations of ocean tides, in *Proceedings of the 9th Int. Symp. Earth Tides,* ed. Kuo, J.T., pp. 341–348, Schweizerbart, Stuttgart.

Baker, T.F. & Bos, M.S., 2003. Validating Earth and ocean tide models using tidal gravity measurements, *Geophys. J. Int.,* **152**(2), 468–485.

Beaumont, C. & Berger, J., 1974. Earthquake prediction: modification of the earth tide tilts and strains, *Geophys. J. R. astr. Soc.,* **39,** 111–121.

Bos, M.S. & Baker, T.F., 2005. An estimate of the errors in gravity ocean tide loading computations, *J. Geod.,* **79**(1–3), 50–63.

Bos, M.S. & Scherneck, H.G., 2014. Free ocean tide loading provider, Available at: http://holt.oso.chalmers.se/loading/, last accessed 5 November 2014.

Calvo, M., Hinderer, J., Rosat, S., Legros, H., Boy, J.-P., Ducarme, B. & Zürn, W., 2014. Time stability of spring and superconducting gravimeters through the analysis of very long gravity records, *J. Geodyn.,* **80,** 20–33.

Carrère, L. & Lyard, F., 2003. Modeling the barotropic response of the global ocean to atmospheric wind and pressure forcing - comparisons with observations, *Geophys. Res. Lett.,* **30**(6), 1275, doi:10.1029/2002GL016473.

Cartwright, D.E., 1972. Secular changes in the oceanic tides at brest, 1711–1936, *Geophys. J. R. astr. Soc.,* **30,** 433–449.

Cartwright, D.E. & Edden, A.C., 1973. Corrected tables of tidal harmonics, *Geophys. J. R. astr. Soc.,* **33,** 253–264.

Cartwright, D.E. & Tayler, R.J., 1971. New computations of the tide-generating potential, *Geophys. J. R. astr. Soc.,* **23,** 45–73.

Cheng, Y. & Andersen, O.B., 2010. Improvement in global ocean tide model in shallow water regions, in *Proceedings of the OSTST Meeting.,* October 18–22, Lisbon.

Chjojnicki, T., 1989. On the variation of tidal wave parameters in time, *Bulletin d'Informations Marées Terrestres,* **105,** 7424–7437.

Dehant, V., 1987. Tidal parameters for an inelastic Earth, *Phys. Earth planet. Inter.,* **49,** 97–116.

Dehant, V., Defraigne, P. & Wahr, J.M., 1999. Tides for a convective Earth, *J. geophys. Res.,* **104,** 1035–1058.

Dittfeld, H.J., 1989. Temporal trends in the variations of tidal parameters, *Bulletin d'Informations Marées Terrestres,* **105,** 7438–7455.
Dittfeld, H.J., 1991. Analysis of Third Degree Waves with Diurnal and Semidiurnal Frequencies, *Bulletin d'Informations Marées Terrestres,* **111,** 8053–8061.
Ducarme, B., 2012. Determination of the main lunar waves generated by the third degree tidal potential and validity of the corresponding body tides models, *J. Geod.,* **86**(1), 65–75.
Ducarme, B., Pálinkáš, V., Meurers, B., Xiaoming, C. & Vaľko, M., 2014. On the comparison of tidal gravity parameters with tidal models in central Europe, *Proc. 17th Int. Symp. On Earth Tides, Warsaw, 15–19 April 2013,* ed. Pagiatakis, S., *J. Geodyn.,* **80,** 12–19.
Eanes, R.J., 1994. Diurnal and semidiurnal tides from TOPEX/POSEIDON altimetry, *EOS, Trans. Am. Geophys. Un.,* **75**(16), 108.
Egbert, G.D. & Erofeeva, L., 2002. Efficient inverse modeling of barotropic ocean tides, *J. Atmos. Oceanic Technol.,* **19**(2), 183–204.
Francis, O., Niebauer, T.M., Sasagawa, G., Klopping, F.J. & Gschwind, J.J., 1998. Calibration of a superconducting gravimeter by comparison with an absolute gravimeter FG5 in Boulder, *Geophys. Res. Lett.,* **25**(7), 1075–1078.
Gräwe, U., Burchard, H., Müller, M. & Schuttelaars, H.M., 2014. Seasonal variability in M2 and M4 tidal constituents and its implications for the coastal residual sediment transport, *Geophys. Res. Lett.,* **41,** 5563–5570.
Hábel, B. & Meurers, B., 2014. A new tidal analysis of superconducting gravity observations in Western and Central Europe, *Contrib Geophys. Geod.,* **44**(1), 1–24.
Hartmann, T. & Wenzel, H.G., 1995a. The HW95 tidal potential catalogue, *Geophys. Res. Lett.,* **22**(24), 3553–3556.
Hartmann, T. & Wenzel, H.G., 1995b. Catalogue HW95 of the tide generating potential, *Bull. Inf. Marées Terrestres,* **123,** 9278–9301.
Hinderer, J., Crossley, D. & Warburton, R.J., 2007. Gravimetric methods—superconducting gravity meters, *Treat. Geophys.,* **3,** 65–122.
Huess, V. & Andersen, O.B., 2001. Seasonal variation in the main tidal constituent from altimetry, *Geophys. Res. Lett.,* **28**(4), 567–570.
Lyard, F., Lefèvre, F., Letellier, T. & Francis, O., 2006. Modelling the global ocean tides: a modern insight from FES2004, *Ocean Dyn.,* **56,** 394–415.
Matsumoto, K., Takanezawa, T. & Ooe, M., 2000. Ocean tide models developed by assimilating TOPEX/POSEIDON altimeter data into hydrodynamical model: a global model and a regional model around Japan, *J. Oceanogr.,* **56,** 567–581.
Merriam, J.B., 1995. Non-linear tides observed with the superconducting gravimeter, *Geophys. J. Int.,* **123,** 529–540.
Métivier, L. & Conrad, C.P., 2008. Body tides of a convecting, laterally heterogeneous, and aspherical Earth, *J. geophys. Res.,* **113,** B11405, doi:10.1029/2007JB005448.
Meurers, B., 2004. Investigation of temporal gravity variations in SG-records, *J. Geodyn.,* **38,** 423–435.
Meurers, B., 2012. Superconducting gravimeter calibration by colocated gravity observations: results from GWR C025, *Int. J. Geophys.,* **2012**, doi:10.1155/2012/954271.
Meurers, B., Van Camp, M. & Pálinkáš, V., 2014. Temporal variation of tidal parameters, in *Proceedings of the EGU General Assembly 2014,* Geophysical Research Abstracts, Vol. 16, EGU2014–13225.
Müller, M., 2011. Rapid change in semi-diurnal tides in the North Atlantic since 1980, *Geophys. Res. Lett.,* **38,** L11602, doi:10.1029/2011GL047312.
Müller, M., Arbic, B.K. & Mitrovica, J.X., 2011. Secular trends in ocean tides: observations and model results, *J. geophys. Res.,* **116,** C05013, doi:10.1029/2010JC006387.
Müller, M., Cherniawsky, J.Y., Foreman, M.G.G. & von Storch, J.S., 2014. Seasonal variation of the M2 tide, *Ocean Dyn.,* **64,** 159–177.
Ray, R.D., 1999. A global ocean tide Model from TOPEX/POSEIDON Altimetry: GOT99.2, NASA Technical Memorandum 209478.
Ray, R.D., 2006. Secular changes of the M2 tide in the Gulf of Maine, *Cont. Shelf. Res.,* **26,** 422–427.
Rosat, S., Boy, J.P., Ferhat, G., Hinderer, J., Amalvict, M., Gegout, P. & Luck, B., 2009. Analysis of a 10-year (1997–2007) record of time-varying gravity in Strasbourg using absolute and superconducting gravimeters: new results on the calibration and comparison with GPS height changes and hydrology, *J Geodyn.,* **48**(3–5), 360–365.
Savcenko, R. & Bosch, W., 2011. EOT11a—a new tide model from multi-mission altimetry, in *Proceedings of the OSTST Meeting*, October 19–21, San Diego.
Schüller, K., 2015. Theoretical basis for Earth Tide analysis with the new ETERNA34-ANA-V4.0 program, *Bull. Inf. Marées Terrestres,* **149,** 12 024–12 061.
Taguchi, E., Stammer, D. & Zahel, W., 2010. Estimation of deep ocean tidal energy dissipation based on the high-resolution data-assimilative HAMTIDE model, *J. geophys. Res* (to be submitted).
Van Camp, M., Wenzel, H.-G., Schott, P., Vauterin, P. & Francis, O., 2000. Accurate transfer function determination for superconducting gravimeters, *Geophys. Res. Lett.,* **27**(1), 37–40.
Van Camp, M., de Viron, O., Métivier, L., Meurers, B. & Francis, O., 2014. The quest for a consistent signal in ground and GRACE gravity time-series, *Geophys. J. Int.,* **197,** 192–201.
Van Camp, M., Meurers, B., de Viron, O. & Forbriger, Th., 2016. Optimized strategy for the calibration of superconducting gravimeters at the one per mille level, *J. Geod.,* **90**(1), 91–99.
Van Dam, T. & Francis, O., 1998. Two years of continuous measurements of tidal and nontidal variations of gravity in Boulder, Colorado, Geophys. Res. Lett., **25**(3), 393–396.
Virtanen, H., Bilker-Koivula, M., Mäkinen, J., Näränen, J., Raja-Halli, A. & Ruotsalainen, H., 2014. Comparison between measurements with the superconducting gravimeter T020 and the absolute gravimeter FG5-221 at Metsähovi, Finland in 2003–2012. *Bull. Inf. Marées Terrestres,* **148,** 11 923–11 928 .
Wenzel, H.G., 1996. The nanogal software: Earth tide data preprocessing package, *Bull. Inf. Marées Terrestres,* **124,** 9425–9439.
Woodworth, P.L., 2010. A survey of recent changes in the main components of the ocean tide, *Cont. Shelf Res.,* **30**(15), 1680–1691.

APPENDIX A: MODULATION AMPLITUDE

Suppose two small tidal constituents with amplitudes B and C with equal frequency difference $\Delta\omega$ around the carrier wave with amplitude A and frequency ω. Supposing all waves being in phase at time $t = 0$ and having the same amplitude factor δ, the time variable gravity $\tilde{g}(t)$ composed by these waves reads as:

$$\tilde{g}(t) = \delta \cdot g(t) = \delta \cdot A \sin\omega t + \delta \cdot B \sin(\omega + \Delta\omega)t + \delta \cdot C \sin(\omega - \Delta\omega)t = \tilde{A} \sin(\omega t + \varphi(t))$$

$$\tilde{A} = \delta\sqrt{A^2 + B^2 + C^2 + 2BC\cos 2\Delta\omega\, t + 2A(B + C)\cos\Delta\omega t}$$

$$\varphi(t) = \operatorname{atan}\left(\frac{(B - C)\sin\Delta\omega t}{A + (B + C)\cos\Delta\omega t}\right)$$

δ would be constant over time. This changes if the satellites are associated with amplitude factors δ_B and δ_C

$$\delta_B = \delta + \Delta\delta_B$$

$$\delta_C = \delta + \Delta\delta_C$$

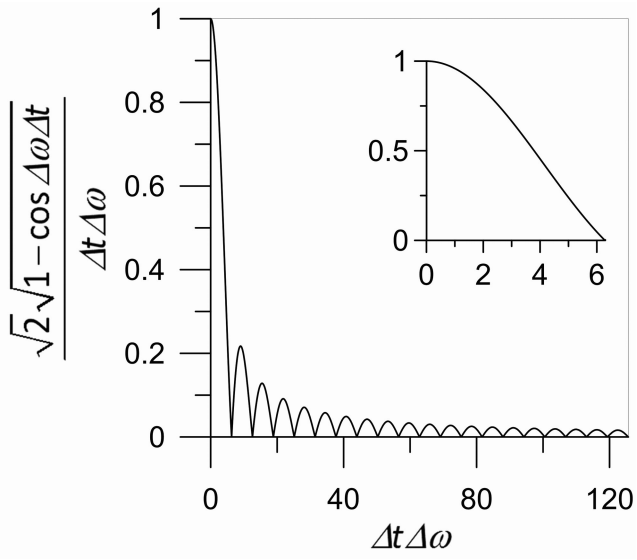

Figure A1. Normalized modulation amplitude $\bar{\delta}_{\mathrm{mod}}$ due to time integration (refer to eq. A1).

with δ_{B} equal or different to δ_{C}. Then the observed gravity $\tilde{g}(t)$ reads as:

$$\tilde{g}(t) = \sqrt{\delta^2A^2 + (\delta+\Delta\delta_B)^2B^2 + (\delta+\Delta\delta_C)^2C^2 + 2BC(\delta+\Delta\delta_B)(\delta+\Delta\delta_C)\cos 2\Delta\omega t + 2\delta\cdot A\,[B(\delta+\Delta\delta_B)+C(\delta+\Delta\delta_C)]\cos\Delta\omega t}\cdot\sin\omega t$$

If B and C are small compared to A, the time variable amplitude factor yields to

$$\begin{aligned}\frac{\tilde{g}(t)}{g(t)} = \delta_{\mathrm{obs}}(t) &= \delta + \frac{1}{2}\frac{\Delta\delta_B^2B^2 + \Delta\delta_C^2C^2}{A^2+B^2+C^2+2BC\cos 2\Delta\omega t + 2A(B+C)\cos\Delta\omega t}\\ &\quad + \frac{BC(\Delta\delta_B+\Delta\delta_C+\Delta\delta_B\Delta\delta_C)\cos 2\Delta\omega t}{A^2+B^2+C^2+2BC\cos 2\Delta\omega t + 2A(B+C)\cos\Delta\omega t} + \frac{A\,(B\Delta\delta_B+C\Delta\delta_C)\cos\Delta\omega t}{A^2+B^2+C^2+2BC\cos 2\Delta\omega t + 2A(B+C)\cos\Delta\omega t}\\ &\cong \delta + \frac{A\,(B\Delta\delta_B+C\Delta\delta_C)\cos\Delta\omega t}{A^2+B^2+C^2+2BC\cos 2\Delta\omega t + 2A(B+C)\cos\Delta\omega t}\\ &= \delta + \delta_{\mathrm{mod}}\cos\Delta\omega t.\end{aligned}$$

Denoting the ratio of B and A by R_{B} and the ratio of C and A by R_{C} we get the modulation amplitude δ_{mod} of the carrier wave:

$$\delta_{\mathrm{mod}} = \frac{R_B\Delta\delta_B + R_C\Delta\delta_C}{1+R_B^2+R_C^2+2R_BR_C\cos 2\Delta\omega t + 2(R_B+R_C)\cos\Delta\omega t} \cong R_B\Delta\delta_B + R_C\Delta\delta_C.$$

Integrating over the period Δt changes the modulation amplitude as follows:

$$\begin{aligned}\frac{1}{\Delta t}\int_t^{t+\Delta t}\delta_{\mathrm{obs}}(\tau)d\tau &\cong \delta + \frac{R_B\Delta\delta_B + R_C\Delta\delta_C}{\Delta t\,\Delta\omega}\left[\sin(\Delta\omega\, t + \Delta\omega\,\Delta t) - \sin\Delta\omega\, t\right]\\ &= \delta + \frac{R_B\Delta\delta_B + R_C\Delta\delta_C}{\Delta t\,\Delta\omega}a\sin(\Delta\omega\, t+\gamma)\\ &\quad \text{with} \qquad a = \sqrt{2}\sqrt{1-\cos\Delta\omega\,\Delta t} \qquad \text{and} \qquad \gamma = \operatorname{atan}\left(\frac{\sin\Delta\omega\,\Delta t}{\cos\Delta\omega\,\Delta t - 1}\right)\end{aligned}$$

$$\frac{1}{\Delta t}\int_t^{t+\Delta t}\delta_{\mathrm{obs}}(\tau)d\tau \cong \delta + \underbrace{(R_B\Delta\delta_B + R_C\Delta\delta_C)\frac{\sqrt{2}\sqrt{1-\cos\Delta\omega\,\Delta t}}{\Delta t\,\Delta\omega}}_{\bar{\delta}_{\mathrm{mod}}}\sin(\Delta\omega\, t+\gamma) \tag{A1}$$

$\bar{\delta}_{\mathrm{mod}}$ corresponds to the effective modulation amplitude of the tidal amplitude factor obtained by analysing successive time-series of length Δt.

Fig. A1 shows the attenuation of the modulation amplitude as a function of the length of the analysed time-series. The modulation amplitude is reduced at least by 80 per cent if the time-series covers two modulation cycles.

Table B1. Largest tidal constituents of the Hartmann & Wenzel (1995a) tidal potential catalogue next to M2. Amplitude normalized with respect to M2. Degree and order of the tidal potential.

	Frequency (cpd)	Normalized amplitude	Degree	Order
GAM2	1.927416706	0.003011	2	2
MA2	1.929535837	0.003448	2	2
255.455	1.931964162	0.000348	3	2
255.545	1.932126522	0.038758	2	2
M2	1.932273616	1	2	2
255.645	1.932435977	0.000055	3	2
255.655	1.932583070	0.000927	3	2
MB2	1.935011395	0.003018	2	2
DLT2	1.937749435	0.001171	2	2

APPENDIX B: TIDAL CONSTITUENTS NEXT TO M2 AND EXAMPLES OF M2 MODULATION

(1) *Annual modulation of M2 by 2nd degree waves MA2, MB2*

If the amplitude factors (and/or phases) of MA2, MB2 were the same as for main M2, modulation would never appear in tidal analyses, even when we do not separate them. MA2, MB2 are represented in the tidal catalogue and thus are modelled in the adjustment approach. Only if the tidal catalogue did not contain MA2, MB2, an annual modulation of the M2 amplitude factor would occur also in this case.

However, if their amplitude factors (and/or phases) differ from main M2, then an annual M2 modulation will appear as long as we do not separate MA2, MB2 from M2, except the analysis interval is an integer multiple of the modulation period (1 yr, see Appendix A).

(2) *2nd degree and 3rd degree waves mixing up within a wave group*

Let the amplitude factor of the body tide be 1.16 for 2nd degree waves and 1.07 for 3rd degree waves. If ocean load causes an increase by a same factor, for example 1.02 for both 2nd and 3rd degree waves, that is 1.16 increases to 1.1832 and 1.07 to 1.0914, then modulation of the M2 amplitude factor will never occur even if we do not separate 2nd and 3rd degree waves.

However, if ocean load causes an increase of the body tide amplitude factor only for 2nd degree waves but does almost not modify 3rd degree waves, then a modulation of the M2 amplitude factor will appear as long as we if we do not separate 2nd and 3rd degree waves. The analysis approach only considers the different elastic body tide response by *a priori* scaling based on the body tide model, which does not know ocean loading. When 3rd degree waves experience no or at least much less loading than 2nd degree waves, then they cause modulation, if they have considerable amplitudes in the tidal spectrum.